HHS Public Access

Author manuscript

Cell Rep. Author manuscript; available in PMC 2016 May 31.

Published in final edited form as:

Cell Rep. 2016 May 24; 15(8): 1728–1742. doi:10.1016/j.celrep.2016.04.052.

An Evolutionarily Conserved PLC-PKD-TFEB Pathway for Host Defense

Mehran Najibi[*,1], **Sid Ahmed Labed**[*,1], **Orane Visvikis**[1,2], and **Javier Elbio Irazoqui**[1,§]

[1]Laboratory of Comparative Immunology, Center for the Study of Inflammatory Bowel Disease, Massachusetts General Hospital Research Institute, Harvard Medical School, Boston, MA, 02114, United States of America

Summary

The mechanisms that tightly control the transcription of host defense genes have not been fully elucidated. We previously identified TFEB as a transcription factor important for host defense, but the mechanisms that regulate TFEB during infection remained unknown. We used *C. elegans* to discover a pathway that activates TFEB during infection. Gene *dkf-1*, which encodes a homolog of protein kinase D (PKD), was required for TFEB activation in nematodes infected with *Staphylococcus aureus*. Conversely, pharmacological activation of PKD was sufficient to activate TFEB. Furthermore, phospholipase C (PLC) gene *plc-1* was also required for TFEB activation, downstream of Gαq homolog *egl-30* and upstream of *dkf-1*. Using reverse and chemical genetics, we discovered a similar PLC-PKD-TFEB axis in *Salmonella*-infected mouse macrophages. In addition, PKCα was required in macrophages but not nematodes. These observations reveal a previously unknown host defense signaling pathway, which has been conserved across one billion years of evolution.

eTOC Blurb

Transcription factor TFEB has recently emerged as a critical regulator of host defense, but the upstream pathway that leads to its activation during infection was unknown. Najibi et al. demonstrate an evolutionarily conserved pathway involving phospholipase C and protein kinase D that is necessary and sufficient for TFEB activation in infected nematodes and macrophages.

[§]to whom correspondence should be addressed: ; Email: jirazoqui@mgh.harvard.edu

[2]Current address: INSERM, U1065, Centre Méditerranéen de Médecine Moléculaire, C3M, Toxines Microbiennes dans la Relation Hôte Pathogènes, Nice, France

[*]these authors contributed equally

Author contributions

All authors designed, analyzed, and interpreted experiments. MN, SAL, and OV performed experiments. All authors contributed to writing the manuscript.

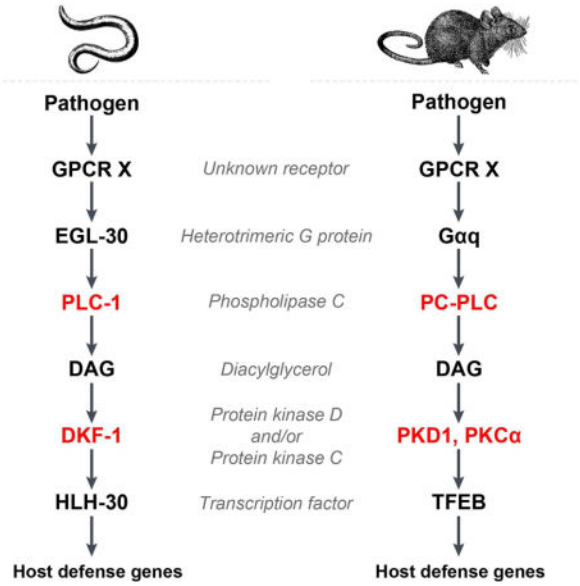

Introduction

Host defense against infection relies on the transcriptional induction of genes that encode antimicrobial proteins and systemic signaling factors (Medzhitov and Horng, 2009). Great strides have been made in understanding the functions of antimicrobials, such as antimicrobial peptides and C-type lectins, and of cytokines and chemokines, such as TNFα, IL1β, and IL6 (Bhatt et al., 2012; Gallo and Hooper, 2012). In contrast, less is understood about the regulatory networks that control their expression during infection, except for a few examples, such as NF-κB (Amit et al., 2009; Shapira and Hacohen, 2011). Host defense gene expression is tightly regulated, and their mis-expression can cause chronic inflammation and autoimmunity (Medzhitov and Horng, 2009). Therefore, understanding transcriptional control of host defense is of great relevance to infectious and inflammatory diseases.

We previously showed that transcription factor EB (TFEB) is an important and evolutionarily-conserved transcriptional regulator of the host response to infection (Visvikis et al., 2014). *Caenorhabditis elegans* TFEB, known as HLH-30, is necessary and sufficient for host defense gene expression. HLH-30 becomes rapidly activated during infection, as revealed by its relocalization from the cytosol to the nucleus of most cells in the organism. Furthermore, TFEB rapidly relocalizes to the nucleus in murine macrophages, where it also is necessary and sufficient for the expression of downstream defense genes. The mechanisms by which nematode and murine TFEB are activated during infection remained unknown.

Previous studies showed that phosphorylation of TFEB by mTORC1 or ERK2 results in its cytoplasmic retention (Peña-Llopis et al., 2011; Roczniak-Ferguson et al., 2012; Sardiello et al., 2009; Settembre et al., 2011). Such inhibition is lifted by nutritional deprivation in nematodes and in mammalian cells (Lapierre et al., 2013; Martina et al., 2012; O'Rourke and Ruvkun, 2013; Settembre et al., 2013). Activated TFEB drives the expression of

lysosomal and autophagy genes that are part of the CLEAR regulatory network (Palmieri et al., 2011), which also includes lipid catabolism genes that are important for cellular metabolic reprogramming (Settembre et al., 2013). Activation of TFEB is much less understood. In nutrient-deprived cells, it entails Ca^{2+}-mediated calcineurin activation, resulting in dephosphorylation of TFEB at mTORC1 target sites and its nuclear import (Medina et al., 2015). Whether this mechanism is involved in TFEB regulation during infection is not known.

Here we report the discovery of an evolutionarily-conserved upstream pathway dependent on protein kinase D (PKD) for the positive regulation of TFEB during infection. In *C. elegans*, PKD homolog DKF-1 is essential for HLH-30 activation during infection. In murine macrophages, we find that PKD activity is also required for TFEB activation during infection, as also is that of PKCα. Thus, our study identifies a role for PKD in innate immune signaling via TFEB in nematodes and mammals, and suggests that PKD and TFEB may perform wider and more central roles in host defense than previously appreciated.

Results

C. elegans DKF-1/protein kinase D is necessary and sufficient for the activation of HLH-30/TFEB

C. elegans possess a TFEB ortholog named HLH-30 (Lapierre et al., 2013; Visvikis et al., 2014). GFP-tagged HLH-30 (HLH-30::GFP) is expressed throughout the body in uninfected animals feeding on nonpathogenic *Escherichia coli*, where it distributes equally between the cellular cytosol and nucleus. In contrast, HLH-30::GFP concentrates in the cell nucleus throughout the entire organism during infection with *Staphylococcus aureus*, indicating that HLH-30 is activated by infection. We observed similar behavior for murine TFEB in macrophages (Visvikis et al., 2014). To clarify upstream regulation of TFEB, we sought to identify candidate signaling molecules that are required for TFEB activation during infection. We used *C. elegans* as a gene discovery tool, with which we screened a library containing RNAi constructs that target most protein kinases and phosphatases in the *C. elegans* genome (Manning, 2005). For the screen, animals were reared on *E. coli* clones expressing dsRNA to each gene individually (see *Methods*). The screen consisted of visual examination of HLH-30::GFP nuclear localization by epifluorescence microscopy after 30 min of *S. aureus* exposure. In this manner, we found that inhibition of gene *dkf-1* prevented HLH-30 nuclear localization during *S. aureus* infection (Fig. 1A, B).

Gene *dkf-1* encodes one of two *C. elegans* homologs of protein kinase D (PKD) (Feng et al., 2006; Fu and Rubin, 2011). Knockdown of *dkf-1* specifically reduced *dkf-1* mRNA by about 50%, but not that of paralagous gene *dkf-2* (Fig. S1A). Furthermore, *dkf-2* RNAi did not affect HLH-30 activation (Fig. 1A, B), suggesting that *dkf-1* specifically controls HLH-30 activation during infection. Consistent with this result, *dkf-1* RNAi knockdown severely compromised host survival of *S. aureus* infection (Fig. 1C). Interestingly, *dkf-1* knockdown in the *hlh-30* mutant background did not impair host survival beyond that of the control *hlh-30* mutant alone ($p > 0.01$, Log-Rank test), which suggested that *dkf-1* and *hlh-30* may function in the same pathway. Non-infected control experiments revealed that inhibition of *dkf-1* resulted in shortened lifespan (Fig. S1B), such as has been shown for *hlh-30* (Lapierre

et al., 2013; Settembre et al., 2013; Visvikis et al., 2014). In contrast, *dkf-1*(ok2695), a partial loss-of-function allele of *dkf-1* that is sufficient to cause posterior body paralysis (Feng et al., 2007) resulted in non-significant reduction of host survival of infection ($p = 0.1277$), likely because paralysis is insufficient to compromise host defense (Fig. S1C). Together these results suggested that DKF-1 performs functions that are essential for HLH-30 activation during infection.

DKF-1 was previously shown to be activated by the second messenger 1,2-diacylglycerol (DAG) in a PKC-independent manner, and can be activated using the DAG analog phorbol 12-myristate 13-acetate (PMA) (Feng et al., 2007). Exogenous addition of PMA was sufficient to induce HLH-30 translocation (Fig. 1D, E) and induction of HLH-30-dependent gene *ilys-2* (Visvikis et al., 2014) (Fig. 1F, G) in the absence of infection. Such effects were diminished as a result of *dkf-1* knockdown (Fig. 1D, E, G), demonstrating that PMA-triggered HLH-30 activation is DKF-1-dependent. Together, these results show that activation of PKD homolog DKF-1 is necessary and sufficient to induce HLH-30 activation.

PMA can also activate protein kinase C (PKC). To test whether PKC might also be involved in HLH-30 activation during infection, we examined the effect of chemical inhibition of PKC on HLH-30 nuclear translocation. Animals that were treated with vehicle alone or with PKC inhibitor Bisindolylmaleimide IV (Jirousek et al., 1996) were indistinguishable (Fig. 1H, I). In stark contrast, treatment with PKD inhibitor kb-NB142-70 (Harikumar et al., 2010) resulted in a 75% inhibition of HLH-30 translocation, supporting the findings with *dkf-1* RNAi. Furthermore, individual loss of of PKC paralagous genes *pkc-1, pkc-2*, and *tpa-1* did not affect HLH-30 translocation (Fig. 1J, K) nor *ilys-2* induction (Fig. S1D). Together, these results support a key role for *dkf-1*, but not *dkf-2* or PKC, in the activation of HLH-30 during infection.

C. elegans EGL-30/$G\alpha_q$ and PLC-1/PLCε are necessary for the activation of HLH-30

We hypothesized that infection may result in increased cellular DAG levels, thus causing PKD activation. A common endogenous source of DAG is phosphatidyl inositide 4,5-bisphosphate (PIP_2), which is hydrolyzed to inositol trisphosphate (IP_3) and DAG by phospholipase C (PLC) (Kadamur and Ross, 2013). PLC can be activated by interaction with α subunits of heterotrimeric Gq proteins, or $G\alpha_q$ (Taylor et al., 1991). Furthermore, previous work showed that the *C. elegans* $G\alpha_q$ homolog EGL-30 can activate PLCβ homolog EGL-8 for host defense against *Pseudomonas aeruginosa* or *Microbacterium nematophilum* infection (Kawli et al., 2010; McMullan et al., 2012). In addition, activation of EGL-30 during fungal infection triggers EGL-8 and Ca^{2+} release to activate dual oxidase, or Duox (Zou et al., 2013). With this precedent in mind, we investigated the role of the EGL-30 – EGL-8 axis in HLH-30 activation by infection.

First, we tested whether EGL-30 might be important for HLH-30 activation. RNAi knockdown of gene *egl-30* resulted in severely defective HLH-30 nuclear localization after infection (Fig. 2A, B). In addition, loss of function *egl-30* mutants were highly susceptible to *S. aureus* infection compared with wild type (Fig. 2C), consistent with the putative role of EGL-30 upstream of PLC.

Next, we addressed whether EGL-8 might also participate in HLH-30 regulation. In this case, RNAi knockdown of gene *egl-8* did not affect HLH-30 (Fig. 2D, E), suggesting that another PLC homolog may be involved. To identify the hypothetical phospholipase that may function upstream of HLH-30 during infection, we performed RNAi-mediated knockdown of additional PLC genes *plc-1, plc-2, plc-3*, and *plc-4*. While animals treated with *plc-2, plc-3*, or *plc-4* RNAi were indistinguishable from empty vector controls, *plc-1* knockdown abrogated HLH-30::GFP nuclear localization (Fig. 2D, E). Unexpectedly, *plc-1* RNAi conferred enhanced survival of infection (Fig. S1E). In contrast, *plc-1* RNAi caused shortened lifespan on nonpathogenic *E. coli* (Fig. S1F); thus, the observed resistance to infection is not explained by an extended lifespan. Loss of *plc-1* has been reported to cause pleiotropic defects in multiple processes, including fertilization (Kovacevic et al., 2013) and morphogenesis (Vázquez-Manrique et al., 2008). In addition, *plc-1* RNAi causes defects in chromosome condensation and embryonic lethality (Vázquez-Manrique et al., 2008). Because PLC-1 participates in numerous organismal functions, the observed lifespan phenotypes could be affected in a complex manner by *plc-1* RNAi. Nonetheless, our finding that PLC-1 is required for HLH-30 nuclear import suggests that PLC-1 is specifically required for HLH-30 activation by infection.

To examine whether EGL-30 and PLC-1 might function upstream of DKF-1, we tested the ability of PMA to suppress the phenotypes caused by their loss of function in terms of HLH-30 activation. PMA caused HLH-30 translocation in animals treated with RNAi against *plc-1* or *egl-30*, but not in those treated *with dkf*-1 RNAi (Fig. 2F, G). This result suggested that DAG produced downstream of EGL-30 and PLC-1 can activate DKF-1 and HLH-30 translocation.

Together, these data suggest a hypothetical model whereby infection triggers an unknown G protein-coupled receptor (GPCR X, Fig. 2H), which could activate PLC-1 via EGL-30 (although more complex indirect scenarios are also possible). PLC-1 generates DAG, which recruits DKF-1 to the membrane, resulting in its activation. Directly or indirectly, activated DKF-1 causes HLH-30 to concentrate in the nucleus, where it can drive the expression of host defense genes such as *ilys-2*. Because HLH-30 and its mammalian homolog TFEB are both regulated by infection, we hypothesized that a similar pathway might operate in mammalian innate immune cells.

Murine PKD1 is necessary and sufficient for TFEB activation in macrophages

To test whether PKD regulates TFEB also in macrophages, we incubated TFEB-GFP RAW264.7 cells with PKD inhibitors. Compounds kb-NB142-70 and CRT0066101 were previously identified as specific PKD antagonists (Harikumar et al., 2010; LaValle et al., 2010). Preincubation with either compound prevented TFEB nuclear translocation upon subsequent *Salmonella* infection (Fig. 3A–C′, G, H, S2A–C′, F, G), indicating that PKD is required for TFEB activation. In addition, CRT0066101 caused ectopic localization of TFEB to unknown structures resembling vesicles (Fig. S2C, C′). Furthermore, shRNA-mediated knockdown showed that genes *Prkd2* and *Prkd3*, encoding PKD2 and PKD3 respectively, were dispensable for TFEB activation by *Salmonella*, while *Prkd1*, encoding PKD1, was absolutely required (Fig. 3I–O). Control experiments showed that *Prkd1* shRNA specifically

reduced expression of PKD1 by about 80% (Fig. 3P, Q). Together, these results suggested that PKD1 activity is required for TFEB activation during infection.

As mentioned, we found that PMA can activate HLH-30 in *C. elegans*, in a manner dependent on PKD homolog DKF-1. To test whether PMA can also activate TFEB through PKD in macrophages, we incubated TFEB-GFP RAW264.7 cells with PMA. Such treatment was sufficient to induce TFEB nuclear translocation in the absence of infection (Fig. 4A–B′, G, H). Furthermore, inhibition of PKD using compounds kb-NB142-70 or CRT0066101 completely abrogated this effect (Fig. 4C–D′, G, H). TFEB electrophoretic mobility changes due to phosphorylation (Visvikis et al., 2014). We noticed subtly altered electrophoretic mobility of TFEB as soon as 10 minutes after PMA incubation, which reverted after 30 min (Fig. 4I, J). In addition, we observed a slight increase in TFEB levels after PMA incubation. Although they do not ascribe the slower mobility to direct phosphorylation of TFEB by PKD, these observations indicate that PKD activation is necessary and sufficient for TFEB nuclear translocation during infection.

Murine PKC is necessary and sufficient for TFEB activation in macrophages

DKF-1 was previously shown to become activated by DAG in a PKC-independent manner (Feng et al., 2007). In contrast, in mammalian cells PKD can also be activated by PKC (Rozengurt, 2011). To test the importance of PKC for TFEB activation, we preincubated TFEB-GFP RAW264.7 cells with selective PKC inhibitors, and subsequently infected them with *Salmonella*. Incubation with Gö 6983 and Bisindolylmaleimide IV, which inhibit all PKC isozymes (Gschwendt et al., 1996; Smith and Hoshi, 2011), abrogated TFEB activation (Fig. 3D, D′, G, H, S2D, D′, F, G). Furthermore, incubation with HBDDE, which inhibits PKCα and PKCγ (Kashiwada et al., 1994), also prevented TFEB activation (Fig. 3E, E′, G, H), whereas incubation with LY333531, which inhibits PKCβ (Jirousek et al., 1996), or PKCε inhibitor peptide (Johnson et al., 1996) did not (Fig. 3F–H, S2E–G). Similar results were obtained in TFEB-Flag-expressing RAW264.7 cells infected with live or dead *S. aureus* (Fig. S3). These results suggested that neither PKCβ, which was previously shown to control TFEB abundance in osteoclasts (Ferron et al., 2013), nor PKCε, which is required for phagocytosis in macrophages (Castrillo et al., 2001; Larsen et al., 2000), were required for TFEB activation by infection. In contrast, PKCα and/or PKCγ are required for TFEB activation during infection.

Similar to PKD, PKC can be activated using PMA (Lin and Chen, 1998). As with PKD inhibitors, HBDDE prevented TFEB activation by PMA, whereas LY333531 did not (Fig. 4E–H). Taken together, these data suggest that DAG generated during infection may result in the activation of PKCα (or PKCγ, but not PKCβ) and PKD1, both of which are required for TFEB nuclear translocation.

PKCα and PKD are quickly activated by infection in macrophages

Our results thus far suggested that PKCα/γ and PKD1 were important for TFEB activation during infection. However, it was not clear whether they played a permissive role for TFEB activation, or if they might actively transduce a signal that triggers TFEB translocation. PKC isozymes are constitutively phosphorylated on specific Ser and Thr residues following

translation, in a process known as 'maturation' (Wu-zhang and Newton, 2013). C-terminal Ser916 phosphorylation of PKD isozymes results in their activation (Kunkel and Newton, 2015). Thus, phosphorylation of specific residues can be used as a measure of PKC maturation and of PKD activation. To address whether PKC and PKD might be differentially regulated during infection, we performed Western blot analysis of lysates from infected RAW264.7 cells. We used antibodies that specifically recognize phosphorylated PKCα/β, PKCδ, PKCδ/θ, PKCζ/λ, and all three PKD isozymes (see *Methods*).

PKCδ and PKCδ/θ phosphorylation did not vary considerably over a 2 hour timecourse (Fig. 5A–C). In contrast, PKCζ/λ phosphorylation decreased fivefold (Fig. 5A, D, E). Furthermore, PKCα/β phosphorylation increased fourfold just 10 min after infection, and remained twofold higher than baseline after 2 hours (Fig. 5A, F, G). In addition, PKD became phosphorylated by 10 min and reached a further threefold higher level after 2 hours (Fig. 5A, H). In contrast, total PKD diminished over time, about tenfold after 2 hours (Fig. 5A, I). TFEB levels remained steady throughout, but its electrophoretic mobility appeared to slightly increase with time (Fig. 5A, J, S4A), consistent with decreased phosphorylation previously observed upon activation and nuclear import (Medina et al., 2015; Visvikis et al., 2014). Furthermore, pre-incubation with PKD inhibitor kb-NB142-70 resulted in increased mobility even at early times of infection (Fig. 5K, L, S4B). Considered together with our previous chemical inhibition results, these experiments suggested that PKCα and PKD are promptly activated after infection and are required for downstream TFEB activation.

Salmonella enterica must be alive to activate the PKD-TFEB pathway in macrophages

Pattern recognition receptors (PRRs), such as Toll-like receptors (TLRs), recognize molecules that form part of bacterial cells, such as LPS. To investigate the potential for such receptors to be involved in TFEB activation, we examined dead *Salmonella*, which possess such molecules and thus should trigger PRRs as well as live *Salmonella*. To our surprise, we found that heat-killed *Salmonella* did not increase PKD phosphorylation (Fig. 6A–C), and thus would not activate PKD. Consistent with this finding, we did not observe TFEB activation during incubation with either heat-killed or antibiotic-killed *Salmonella* (Fig. 6D–I). Therefore, we concluded that under these conditions the PKD-TFEB pathway specifically responds to live *Salmonella*.

PC-PLC is required for TFEB activation in macrophages

PKCα and PKD are activated by DAG. As mentioned, intracellular DAG is generated by the action of PLC. Therefore, we hypothesized that PLC may be required for activation of PKCα and PKD upstream of TFEB. In support of this hypothesis, we had found that *C. elegans* PLC homolog PLC-1 is required for the activation of TFEB homolog HLH-30, as mentioned previously. To further test this hypothesis, we examined the effect of PLC inhibitors on TFEB activation by infection. Inhibition of phosphoinositide (PI)-PLC using U-73122 (Bleasdale et al., 1990), or of phospholipases D1 and 2 (PLD1 and PLD2) using VU0359595, CAY10594, FIPI, or Halopemide (Lewis et al., 2009; Monovich et al., 2007; Scott et al., 2009; Su et al., 2009) did not affect TFEB activation (Fig. 7D–J). In contrast, inhibition of phosphatidylcholine (PC)-PLC using D609 (Amtmann, 1996) effectively prevented TFEB nuclear translocation (Fig. 7A–C′, I, J). Therefore, PC-PLC activity is

required for TFEB activation during infection, presumably by generating DAG and thus activating PKCα and PKD. To further test this idea, we measured PKD activation by *Salmonella* in D609-treated macrophages, by anti-phospho-PKD immunoblot. Unfortunately, inhibition of PC-PLC resulted in constitutive phosphorylation of PKD, even in the absence of infection (t = 0 min, Fig. 7K, L). Thus, it was not possible to assess the effect of D609 during infection-induced phosphorylation of PKD. Taken together, these observations suggest that the activity of mammalian TFEB is controlled by a PLC-PKD cascade, as discovered using *C. elegans* (Fig. 7M). By analogy with nematodes, it is possible that $G\alpha_q$ mediates activation of this cascade by an unknown GPCR in macrophages.

Discussion

Our previous work established that TFEB is activated during infection in nematodes and macrophages, suggesting that TFEB is an evolutionarily ancient component of host defense (Visvikis et al., 2014). TFEB activation was required for the induction of host defense genes in both nematodes and mammals (Visvikis et al., 2014). Subsequent independent work showed that LPS can stimulate TFEB, with important consequences for antigen presentation by DCs (Samie and Cresswell, 2015). Furthermore, activation of TFEB was shown to be important for host defense against staphylococcal pore forming toxins (Maurer et al., 2015). Thus, the question of how TFEB is regulated during infection is relevant to many aspects of host defense and inflammation. Previous work established that phosphorylation of TFEB by mTORC1 and by ERK2 resulted in its cytoplasmic retention (Martina et al., 2012; Peña-Llopis et al., 2011; Sardiello et al., 2009), and that such negative regulation was lifted during starvation stress by the action of protein phosphatase calcineurin (Medina et al., 2015). However, to date no positive regulatory interaction had been described. Furthermore, the upstream pathways important for TFEB activation specifically during infection were unknown.

Here we showed that a PLC-PKD pathway is necessary and sufficient for TFEB activation in nematodes and in mouse macrophages infected with *Salmonella* or *S. aureus*. An unbiased *in vivo* reverse genetic screen performed using *C. elegans* revealed the requirement of PKD homolog DKF-1 for HLH-30 activation by infection, which led us to discover that PLCε homolog PLC-1 and $G\alpha_q$ homolog EGL-30 are also required.

These results suggest a hypothetical model in which infection activates $G\alpha_q$, presumably via an unidentified G-protein coupled receptor (GPCR X, Fig. 7K). $G\alpha_q$ activates PLCε, which generates DAG, resulting the activation of PKD. PKD activation is required for TFEB nuclear translocation, and downstream transcription of host defense genes. Recent evidence supports a role for PLC-1 downstream of EGL-30 for salt chemotaxis as well (Kunitomo et al., 2013). We observed a complex phenotype for knockdown of *plc-1*. The products of PLC-1 activity, IP3 and DAG, feed into many pathways, complicating the evaluation of the relationship between the observed survival phenotypes and HLH-30. This area requires further exploration. However, the one phenotype that is specific to HLH-30, its nuclear localization during infection, is clearly dependent on PLC-1. This pathway resembles a previously described pathway for epidermal transcription of antimicrobial peptides following infection by fungal pathogen *Drechmeria coniospora*. In such pathway, a GPCR-

$G\alpha_{12}$-PLCγ-PKCδ pathway controls a STAT-type transcription factor (Dierking et al., 2011; Ziegler et al., 2009; Zugasti et al., 2014). *C. elegans* $G\alpha_q$ also has known roles upstream of PLCβ for the regulation of host defense against *P. aeruginosa* and oxidative stress (Kawli et al., 2010) and for the upregulation of transcription factor DAF-16 in the epidermis during *D. coniospora* infection (Zou et al., 2013). Furthermore, *C. elegans* $G\alpha_q$ was recently shown to control both innate immunity and infection avoidance behavior against *M. nematophilum* (McMullan et al., 2012). In addition, DKF-2, which is paralogous to DKF-1, is controlled by PKCδ and is important in the intestine for p38 MAPK-mediated defense against *Enterococcus faecalis* and *P. aeruginosa* through dual oxidase (Duox) BLI-3 (Feng et al., 2007; van der Hoeven et al., 2011, 2012; Ren et al., 2009). Whether DKF-1 is also important for HLH-30 activation in animals infected with *Enterococcus faecalis* or *P. aeruginosa*, or whether this might be dependent on DKF-2 instead, remains to be determined. Activation of DAF-16 by *D. coniospora* in the epidermis also requires Ca^{2+} release and BLI-3 (Zou et al., 2013). Thus, the potential involvement of Ca^{2+} and Duox in TFEB activation during infection deserves further investigation in nematodes and mammals.

We find that key aspects of the proposed *C. elegans* GPCR-$G\alpha_q$-PLCε-PKD-TFEB pathway are conserved in mouse macrophages, where PLC, PKD1, and PKCα are all required for TFEB activation by *Salmonella*. Murine PKCα and PKD are rapidly activated following *Salmonella* infection, and PMA-mediated stimulation of PKC and/or PKD is sufficient to activate TFEB and downstream gene transcription in nematodes. These results are consistent with previous observations that PKC is quickly activated in infected macrophages (Knethen and Brüne, 2005), that PKCα is required for the respiratory burst (Larsen et al., 2000), and that PKD can induce autophagy (Eisenberg-Lerner and Kimchi, 2012). Previous observations that PMA activates TFEB in HEK293 cells lend further support (Huan et al., 2005). We were unable to use PC-PLC inhibitor D609 to test whether PKD activation is PLC-dependent, because D609 incubation led to constitutive PKD phosphorylation. Although the exact mechanism is unknown, we suspect that a compensatory mechanism is activated by tonic PC-PLC inhibition, which could lead to constitutive PKD S916 phosphorylation (but not TFEB translocation). Because inhibition of *C. elegans* gene *plc-1* also yielded unexpected results, this topic is of great interest for future study. Taken together, our findings demonstrate a PKD- and TFEB-dependent mechanism of transcriptional regulation in response to infection, which is evolutionarily ancient. It will be interesting to determine under what other circumstances TFEB mediates PKD signaling.

PKC and PKD have been shown to regulate each other in other systems (Rozengurt, 2011). Furthermore, recent studies have implicated PKD1 as an important signaling molecule downstream of TLR signaling through scaffold protein MyD88 in macrophages and dendritic cells (Kim et al., 2010; Park et al., 2008, 2009). After stimulation with TLR ligands such as LPS and flagellin, the production of TNFα requires PKD1. In cells depleted of PKD1, TRAF6 fails to become ubiquitylated, effectively interrupting signal transduction to transcription factor NF-κB (Park et al., 2009). Our results indicate that in addition to this known role in TLR-MyD88-NF-κB signaling, PKD plays an important role in signaling to TFEB. Our results are consistent with direct signaling to TFEB by PKD1. In addition, TFEB phosphorylation is PKD-dependent in cytotoxic T cells (Navarro et al., 2014), and our bioinformatic analysis of the TFEB amino acid sequence revealed a putative PKD consensus

phosphorylation site in the TFEB N-terminus. However, we cannot presently rule out intermediate steps linking PKD1 to TFEB. For example, PKD can activate the MAPK ERK in endothelial cells (Wong and Jin, 2005). Nonetheless, in our system MEK inhibitors did not prevent TFEB activation by infection (MN and JEI, unpublished data), suggesting that ERK signaling may not be required. Still, some other unknown signaling component could link PKD to TFEB.

Exactly how TFEB becomes activated during infection is not well understood. TFEB abundance is positively regulated through C-terminal phosphorylation by PKCβ in differentiated osteoclasts, as part of a pathway downstream of RANKL signaling (Ferron et al., 2013). However, in that study phosphorylation by PKCβ did not affect TFEB localization. Furthermore, we directly tested the role of PKCβ in activation of TFEB by infection. Inhibition of PKCβ using LY333531 did not prevent TFEB activation by *Salmonella* nor PMA, indicating that PKCβ is not required in these scenarios. Thus, TFEB abundance, subcellular localization, and transcriptional activity are subject to complex regulation in different cell types under distinct circumstances. Further study is required to test the relevance of such regulatory interactions in the context of host-pathogen interactions, and to elucidate the mechanistic basis of TFEB activation during infection. Answering these questions will provide important insights into what are likely to be fundamental mechanisms of host-microbe interaction in many organisms.

Experimental Procedures

Bacterial strains

Escherichia coli OP50 is a gift from Gary Ruvkun, Massachusetts General Hospital (MGH) Research Institute, USA. *Salmonella enterica* serovar *Typhimurium* SL1344 is a gift from Brian Coombes (McMaster University, Canada). *Staphylococcus aureus* NCTC8325 and SH1000 (a functional *rsbU+* derivative of 8325-4 *rsbU*⁻) are a gift from Fred Ausubel, MGH Research Institute, USA.

C. elegans strains

C. elegans were grown on nematode-growth media (NGM) plates seeded with *E. coli* OP50 according to standard procedures (Powell and Ausubel, 2008). *C. elegans* strains used in this study: N2 Bristol wild type (CGC), VT1584 *hlh-30*(tm1978)IV (CGC), RB2037 *dkf-1*(ok2695)I (CGC), JIN1693 *hlh-30*(tm1978); jinIs10 [*hlh-30p::hlh-30::gfp,rol-6*(su1006)].

C. elegans qRT-PCR

After infection, *C. elegans* were washed twice in cold water and lysed in TRI Reagent (Molecular Research Center). cDNA was obtained with SuperScript III (Invitrogen) and analyzed as in (Irazoqui et al., 2008). Data analysis was performed using the Pfaffl method (Pfaffl, 2001).

C. elegans infection

S. aureus SH1000 was grown overnight in tryptic soy broth (TSB) containing 50 μg/ml kanamycin (KAN). 10 μl of overnight (ON) cultures was uniformly spread on the entire surface of 35 mm trypticase soy agar (TSA) plates with 10 μg/ml KAN, and incubated 4–6 h at 37 °C. RNAi-treated L4 larvae were first transferred onto new HT115 RNAi plates supplemented with 80–100 μg/ml 5-fluoro-2′-deoxyuridine (FUDR) for 24 h at 15 °C before transfer to *S. aureus* plates. After FUDR treatment, 25 – 40 infertile animals were transferred to each of three replicate infection plates per strain. Animals that died of bursting vulva, matricidal hatching, or crawling off the agar were censored. Experiments were performed at least twice.

RNAi by feeding

RNAi was carried out using bacterial feeding RNAi (Timmons et al., 2001). HT115 RNAi clones were obtained from the Ahringer genomic RNAi library, or the Vidal library when absent in the former. Clone identity was confirmed by sequencing, and absence of off target effects was verified against predictions by the *C. elegans* genomic database resource, WormBase (www.wormbase.org) and by qRT-PCR. For *dkf-1* gene knockdown, young adults were incubated 4 days at 15 °C on *E. coli* HT115 RNAi plates, so that the progeny was exposed to dsRNA from embryo to L4 stage.

PMA treatment of *C. elegans*

PMA treatment was performed on NGM plates supplemented with 1 μg/ml PMA (Sigma). HLH-30::GFP animals were treated at the young adult stage and incubated at room temperature with and without PMA. After 30 min the animals were harvested and prepared for imaging.

Longevity assays

All assays were performed at 25 °C as described in (Powell and Ausubel, 2008). Animals were transferred by picking to NGM + OP50 plates supplemented with 80 – 100 μg/ml FUDR and incubated at 25 °C. Experiments were performed at least twice. Kaplan-Meier survival analyses were performed using software Prism 5 (GraphPad). Survival data were compared using the Log-Rank significance test.

C. elegans preparation for imaging

L4 animals expressing HLH-30::GFP were grown on NGM plates for 24 h at 15 °C, then kept for 2 h at room temperature, before transfer 30 min prior to imaging onto *S. aureus* killing assay plates, PMA plates, or NGM plates used as control. Animals were harvested by washing with M9W buffer (Powell and Ausubel, 2008), and paralyzed with 10% NaN_3 in 96-well plates. Image acquisition was automatically performed using a Cytation 3 Imaging Plate Reader (Biotek).

Statistical analysis

Statistical analyses were performed using Prism 5 software (GraphPad). Survival data were compared using the Log-Rank test. Data are represented as median survival (MS), as defined

by Kaplan-Meier analysis, or Time to 50% Death (LT_{50}), as defined by nonlinear regression. A p value ≤ 0.05 was considered significantly different from control. For qRT-PCR, two-sample, two-tailed *t* test statistical analyses were performed to evaluate differences among pooled ΔCt values according to Pfaffl (Pfaffl, 2001) using Excel. A p value ≤ 0.05 was considered significant. For imaging quantification, two-sample, two-tailed *t* test statistical analyses were performed. Before use of the *t*-test, all values were confirmed for normal distribution by the Agostino Pearson omnibus test.

Cell culture and transfection

RAW264.7 macrophages were grown in DMEM high glucose, GlutaMAX (Life Technologies 10566-024) containing 10% FBS (Life Technologies 10082147) 1% Antibiotic-Antimycotic (Life Technologies 15240-062). Cells were passage 4 to 11. RAW264.7 TFEB-GFP stably transfected cells were created using pEGFP-N1-TFEB (a gift from Shawn Ferguson, Addgene plasmid # 38119), Lipofectamine LTX Reagent with PLUS Reagent (Life Technologies, A12621) according to manufacturer's instructions, and G418 sulfate (Life Technologies, 10131). Ten days after selection, stable GFP+ cells were separated by FACS. RAW264.7 cells stably expressing TFEB-flag were a gift from Mathieu Ferron (Institut de Recherches Cliniques de Montréal, Canada) (Ferron et al., 2013). For drug screening we used ViewPlate-96 well black opaque plates (Perkin Elmer 6005182). 6×10^4 cells were seeded in each well. At the end of the experiments, cells were fixed using 4% paraformaldehyde (Sigma-Aldrich, 158127) and incubated with Hoechst stain (Anaspec, AS-83218) at room temperature for 20 minutes as nuclear staining. Image acquisition was automatically performed using a Cytation 3 Imaging Plate Reader (Biotek).

shRNA Knockdown

Lentiviral shRNA plasmids were purchased from Dharmacon RNAi Technologies. PKD1: Gene set: GIPZ Prkd1 shRNA: RMM4532-EG18760. PKD2: Gene set: GIPZ Prkd2 shRNA: RMM4532-EG101540. PKD3: Gene set: GIPZ Prkd3 shRNA: RMM4532-EG75292. After plasmid preparation and diagnostic restriction enzyme digest, we used Lipofectamine 3000 (Thermo Fisher Scientific) for transfection according to manufacturer's instructions. For selection we used 3 μg/ml of puromycin (Sigma-Aldrich) based on previously preformed killing curves. Transfected cells were further purified using FACS. We confirmed knockdown efficiency by Western blot.

Nuclear localization quantification (cells)

Quantification of nuclear localization % was performed automatically using Biotek Gen5 Data Analysis Software. First we measured total cell numbers by finding objects positive for the nuclear dye (Hoechst). Next, we identified cells that exhibited higher GFP intensity in the nucleus than in the cytosol, and thus calculated the percent of cells that exhibited nuclear localized TFEB (nuclear localization %). We reckon that this method likely provides an underestimate of nuclear localization, because nuclear GFP was harder to detect automatically in cells that express low levels of TFEB-GFP. The N/C ratio was measured using CellProfiler version 2.1.1 (Broad Institute), as in (Carpenter et al., 2006; Han et al., 2011; Jones et al., 2008).

Infection *in vitro*

Bacteria were grown overnight at 37 °C in LB medium (Difco, BD) with 100 μg/ml streptomycin for *Salmonella* and Columbia medium (Difco, BD) with 10 μg/ml Nalidixic acid for *S. aureus*. The following day, cultures were diluted 1:50 in the same medium and grown at 37 °C for 3 h to late-exponential phase, washed twice in cold PBS, and cells were infected at MOI 10 for *S. aureus and* MOI 100 for *S. enterica*, as in (Trieu et al., 2009; Van Engelenburg and Palmer, 2010; Visvikis et al., 2014). For experiments using heat-killed pathogen, bacteria were heated to 75 °C for 1 h and 100% killing was confirmed by culture for 48 h on LB-streptomycin agar at 37°C. For gentamycin antibiotic (AB) – killed bacteria, before addition to RAW264.7 cells, gentamicin (100 μg/ml) was added to washed bacteria in PBS for 2 hours and 100% killing was confirmed by culture for 48 h on LB-streptomycin agar at 37°C. The appropriate amount of bacteria was resuspended in DMEM 10% FBS without antibiotic and cells were infected with indicated amounts of bacteria.

Immunofluorescence

RAW264.7 TFEB-Flag cells were seeded in 12-well plates containing NUNC Thermanox coverslips. After treatment, cells were fixed with 4% paraformaldehyde (PFA) pH 7.4 at room temperature for 10 min and washed 3 times in PBS (Gibco Life Technologies, 10010) for 5 min each. PFA was neutralized with 50 mM NH_4Cl in PBS at room temperature for 10 min with agitation. After 3 washes with PBS, cells were permeabilized with 0.1% Triton X in PBS at room temperature on agitator for 5 min and then blocked with 5% bovine serum albumin (Sigma-Aldrich, A9647) in PBS for 1 h. After 3 washes with PBS, cells were incubated with 1:400 monoclonal anti-FLAG antibody (Sigma-Aldrich, F1804) in humid chamber for 1 h. Cells were washed three times in PBS and incubated with the fluorescent secondary antibody plus Hoechst stain (Anaspec, AS-83218) at room temperature in humid chamber for 1 h. After using prolong anti-fade reagent (Life Technologies, P7481) as mounting media, coverslips were stored at 4 °C until image acquisition using a Cytation 3 imaging plate reader.

Immunoblotting

After time course of infection with *Salmonella enterica* serovar *Typhimurium* SL1344, RAW264.7 cells were washed 3 times with PBS, harvested, and lysed with 1X SDS sample buffer Blue Loading Pack (Cell Signaling, 7722) at 100 μl per well of 6-well plate. Lysates were heated at 100 °C for 5 min and then centrifuged for 5 min. The supernatant was collected and sonicated, gel electrophoresis was performed using NuPAGE® Novex® 4–12% Bis-Tris Protein Gels (Life Technologies, NP0327), and then transferred onto nitrocellulose (Life Technologies, LC2009). After wash with TBS (Life Technologies, 28358) for 5 minutes, membranes were soaked in blocking buffer containing 1X TBS with 5% BSA for 1 hour at room temperature. After 3 washes with TBS-Tween (Life Technologies, 28360), membranes were incubated overnight at 4 °C with primary antibodies and gentle agitation. Next membranes were washed three times with TBS-Tween and incubated with HRP-conjugated secondary antibody (Cell Signaling, 7074 1:2000) for 1 h at room temperature with gentle agitation. Membranes were then washed with TBS-Tween and incubated with LumiGLO® (Cell signaling, 7003) for 1 min and exposed to x-ray film

(Denville Scientific, E3012). Quantification of western blotting was performed by ImageJ software (U.S. National Institutes of Health, Bethesda, MD, USA). The total level of protein of interest was normalized to β-Actin protein as control. Primary antibodies and dilutions were as follows: β-actin antibody (Cell Signaling Technology, 4967, 1:1000), TFEB antibody (Bethyl Laboratories, A303-673A, 1:2000), PKD1 + PKD2 + PKD3 antibody (Life Technologies, PA5-36113, 1:1000), Phospho-PKD (Ser916) antibody (Cell Signaling Technology 2051, 1:1000), Phospho-PKCα/β II (Thr638/641) antibody (Cell Signaling Technology 9375, 1:1000), PKCα Antibody (Cell Signaling Technology, 2056, 1:1000), Phospho-PKCζ/λ (Thr410/403) antibody (Cell Signaling Technology, 9378, 1:1000), Phospho-PKCδ (Thr505) antibody (Cell Signaling Technology, 9374, 1:1000), Phospho-PKCδ/θ (Ser643/676) antibody (Cell Signaling Technology 9376, 1:1000).

Drugs and reagents

Bisindolylmaleimide IV (Cayman Chemical Item Number 13299, 5 μM): pan-PKC inhibitor, HBDDE (abcam, ab141573, 1 mM): Selective PKCα and PKCγ inhibitor, kb-NB142-70 (abcam, ab141773, 10 μM): Selective PKD inhibitor, CRT0066101 (abcam, ab144637, 5 μM): selective PKD inhibitor, LY333531 (Cayman Chemical, 13964, 10 μM): selective inhibitor of PKCβ1 and PKCβ2, PKCε inhibitor peptide (Cayman Chemical, 13964, 10 μM): selective PKCε inhibitor, D609 (Cayman Chemical, 13307, 50 μM): Phosphatidylcholine-specific phospholipase C (PC-PLC) inhibitor, U-73122 hydrate (Sigma-Aldrich, U6756, 50 μM): phosphoinositide-specific phospholipase C (PI-PLC) inhibitor, CAY10594 (Cayman Chemical, 13207, 10 μM): selective Phospholipase D2 (PLD2) inhibitor, VU0359595 (Cayman Chemical, 10955, 10 μM): selective Phospholipase D1 (PLD1) inhibitor, Halopemide (Cayman Chemical, 13205, 10 μM): Phospholipase D1 and Phospholipase D2 Inhibitor.

Supplementary Material

Refer to Web version on PubMed Central for supplementary material.

Acknowledgments

We are grateful for generous intellectual input and technical help provided by Kate Jeffrey (MGH), Christian Reinecker (MGH), Megha Basavappa (MGH), Tatsushi Omatsu (MGH), and three anonymous reviewers. *Caenorhabditis elegans* strains were provided by the CGC, which is funded by National Institutes of Health Office of Research Infrastructure Programs (P40 OD010440). The content is solely the responsibility of the authors and does not necessarily represent the official views of the National Institutes of Health.

References

Amit I, Garber M, Chevrier N, Leite AP, Donner Y, Eisenhaure T, Guttman M, Grenier JK, Li W, Zuk O, et al. Unbiased reconstruction of a mammalian transcriptional network mediating pathogen responses. Sci N Y NY. 2009; 326:257–263.

Amtmann E. The antiviral, antitumoural xanthate D609 is a competitive inhibitor of phosphatidylcholine-specific phospholipase C. Drugs Exp Clin Res. 1996; 22:287–294. [PubMed: 9034754]

Bhatt DM, Pandya-Jones A, Tong AJ, Barozzi I, Lissner MM, Natoli G, Black DL, Smale ST. Transcript Dynamics of Proinflammatory Genes Revealed by Sequence Analysis of Subcellular RNA Fractions. Cell. 2012; 150:279–290. [PubMed: 22817891]

Bleasdale JE, Thakur NR, Gremban RS, Bundy GL, Fitzpatrick FA, Smith RJ, Bunting S. Selective inhibition of receptor-coupled phospholipase C-dependent processes in human platelets and polymorphonuclear neutrophils. J Pharmacol Exp Ther. 1990; 255:756–768. [PubMed: 2147038]

Carpenter AE, Jones TR, Lamprecht MR, Clarke C, Kang IH, Friman O, Guertin DA, Chang JH, Lindquist RA, Moffat J, et al. CellProfiler: image analysis software for identifying and quantifying cell phenotypes. Genome Biol. 2006; 7:R100. [PubMed: 17076895]

Castrillo A, Pennington DJ, Otto F, Parker PJ, Owen MJ, Boscá L. Protein kinase Cepsilon is required for macrophage activation and defense against bacterial infection. J Exp Med. 2001; 194:1231–1242. [PubMed: 11696589]

Dierking K, Polanowska J, Omi S, Engelmann I, Gut M, Lembo F, Ewbank JJ, Pujol N. Unusual Regulation of a STAT Protein by an SLC6 Family Transporter in C. elegans Epidermal Innate Immunity. Cell Host Microbe. 2011; 9:425–435. [PubMed: 21575913]

Eisenberg-Lerner A, Kimchi A. PKD is a kinase of Vps34 that mediates ROS-induced autophagy downstream of DAPk. Cell Death Differ. 2012; 19:788–797. [PubMed: 22095288]

Feng H, Ren M, Wu SL, Hall DH, Rubin CS. Characterization of a Novel Protein Kinase D CAENORHABDITIS ELEGANS DKF-1 IS ACTIVATED BY TRANSLOCATION-PHOSPHORYLATION AND REGULATES MOVEMENT AND GROWTH IN VIVO. J Biol Chem. 2006; 281:17801–17814. [PubMed: 16613841]

Feng H, Ren M, Chen L, Rubin CS. Properties, regulation, and in vivo functions of a novel protein kinase D: Caenorhabditis elegans DKF-2 links diacylglycerol second messenger to the regulation of stress responses and life span. J Biol Chem. 2007; 282:31273–31288. [PubMed: 17728253]

Ferron M, Settembre C, Shimazu J, Lacombe J, Kato S, Rawlings DJ, Ballabio A, Karsenty G. A RANKL-PKCβ-TFEB signaling cascade is necessary for lysosomal biogenesis in osteoclasts. Genes Dev. 2013; 27:955–969. [PubMed: 23599343]

Fu Y, Rubin CS. Protein kinase D: coupling extracellular stimuli to the regulation of cell physiology. EMBO Rep. 2011; 12:785–796. [PubMed: 21738220]

Gallo RL, Hooper LV. Epithelial antimicrobial defence of the skin and intestine. Nat Rev Immunol. 2012; 12:503–516. [PubMed: 22728527]

Gschwendt M, Dieterich S, Rennecke J, Kittstein W, Mueller HJ, Johannes FJ. Inhibition of protein kinase C mu by various inhibitors. Differentiation from protein kinase c isoenzymes. FEBS Lett. 1996; 392:77–80. [PubMed: 8772178]

Han F, Liang P, Wang F, Zeng L, Zhang B. Automated analysis of time-lapse imaging of nuclear translocation by retrospective strategy and its application to STAT1 in HeLa cells. PloS One. 2011; 6:e27454. [PubMed: 22125613]

Harikumar KB, Kunnumakkara AB, Ochi N, Tong Z, Deorukhkar A, Sung B, Kelland L, Jamieson S, Sutherland R, Raynham T, et al. A Novel Small-Molecule Inhibitor of Protein Kinase D Blocks Pancreatic Cancer Growth In vitro and In vivo. Mol Cancer Ther. 2010; 9:1136–1146. [PubMed: 20442301]

van der Hoeven R, McCallum KC, Cruz MR, Garsin DA. Ce-Duox1/BLI-3 Generated Reactive Oxygen Species Trigger Protective SKN-1 Activity via p38 MAPK Signaling during Infection in C. elegans. PLoS Pathog. 2011; 7:e1002453. [PubMed: 22216003]

van der Hoeven R, McCallum KC, Garsin DA. Speculations on the activation of ROS generation in C. elegans innate immune signaling. Worm. 2012; 1:160–163. [PubMed: 24058842]

Huan C, Sashital D, Hailemariam T, Kelly ML, Roman CAJ. Renal carcinoma-associated transcription factors TFE3 and TFEB are leukemia inhibitory factor-responsive transcription activators of E-cadherin. J Biol Chem. 2005; 280:30225–30235. [PubMed: 15994295]

Irazoqui JE, Ng A, Xavier RJ, Ausubel FM. Role for beta-catenin and HOX transcription factors in Caenorhabditis elegans and mammalian host epithelial-pathogen interactions. Proc Natl Acad Sci U S A. 2008; 105:17469–17474. [PubMed: 18981407]

Jirousek MR, Gillig JR, Gonzalez CM, Heath WF, McDonald JH, Neel DA, Rito CJ, Singh U, Stramm LE, Melikian-Badalian A, et al. (S)-13-[(Dimethylamino)methyl]-10,11,14,15-tetrahydro-4,9:16,21-dimetheno-1H,13H-dibenzo[e,k]pyrrolo[3,4-h] [1,4,13]oxadiazacyclohexadecene-1,3(2H)-dione (LY333531) and Related Analogues: Isozyme Selective Inhibitors of Protein Kinase Cβ. J Med Chem. 1996; 39:2664–2671. [PubMed: 8709095]

Johnson JA, Gray MO, Chen CH, Mochly-Rosen D. A protein kinase C translocation inhibitor as an isozyme-selective antagonist of cardiac function. J Biol Chem. 1996; 271:24962–24966. [PubMed: 8798776]

Jones TR, Kang IH, Wheeler DB, Lindquist RA, Papallo A, Sabatini DM, Golland P, Carpenter AE. CellProfiler Analyst: data exploration and analysis software for complex image-based screens. BMC Bioinformatics. 2008; 9:482. [PubMed: 19014601]

Kadamur G, Ross EM. Mammalian Phospholipase C. Annu Rev Physiol. 2013; 75:127–154. [PubMed: 23140367]

Kashiwada Y, Huang L, Ballas LM, Jiang JB, Janzen WP, Lee KH. New hexahydroxybiphenyl derivatives as inhibitors of protein kinase C. J Med Chem. 1994; 37:195–200. [PubMed: 8289196]

Kawli T, Wu C, Tan MWW. Systemic and cell intrinsic roles of Gqalpha signaling in the regulation of innate immunity, oxidative stress, and longevity in Caenorhabditis elegans. Proc Natl Acad Sci U S A. 2010; 107:13788–13793. [PubMed: 20647387]

Kim YI, Park JE, Brand DD, Fitzpatrick EA, Yi AK. Protein kinase D1 is essential for the proinflammatory response induced by hypersensitivity pneumonitis-causing thermophilic actinomycetes Saccharopolyspora rectivirgula. J Immunol Baltim Md 1950. 2010; 184:3145–3156.

Knethen AV, Brüne B. PKCα Depletion in RAW264.7 Macrophages Following Microbial/IFNγ Stimulation Is PC-PLC-Mediated. Antioxid Redox Signal. 2005; 7:1217–1222. [PubMed: 16115026]

Kovacevic I, Orozco JM, Cram EJ. Filamin and Phospholipase C-ε Are Required for Calcium Signaling in the Caenorhabditis elegans Spermatheca. PLoS Genet. 2013; 9:e1003510. [PubMed: 23671426]

Kunitomo H, Sato H, Iwata R, Satoh Y, Ohno H, Yamada K, Iino Y. Concentration memory-dependent synaptic plasticity of a taste circuit regulates salt concentration chemotaxis in Caenorhabditis elegans. Nat Commun. 2013; 4

Kunkel MT, Newton AC. Protein Kinase D Inhibitors Uncouple Phosphorylation from Activity by Promoting Agonist-Dependent Activation Loop Phosphorylation. Chem Biol. 2015; 22:98–106. [PubMed: 25556943]

Lapierre LR, De Magalhaes Filho CD, McQuary PR, Chu CC, Visvikis O, Chang JT, Gelino S, Ong B, Davis AE, Irazoqui JE, et al. The TFEB orthologue HLH-30 regulates autophagy and modulates longevity in Caenorhabditis elegans. Nat Commun. 2013; 4:2267. [PubMed: 23925298]

Larsen EC, DiGennaro JA, Saito N, Mehta S, Loegering DJ, Mazurkiewicz JE, Lennartz MR. Differential requirement for classic and novel PKC isoforms in respiratory burst and phagocytosis in RAW 264.7 cells. J Immunol Baltim Md 1950. 2000; 165:2809–2817.

LaValle CR, Bravo-Altamirano K, Giridhar KV, Chen J, Sharlow E, Lazo JS, Wipf P, Wang QJ. Novel protein kinase D inhibitors cause potent arrest in prostate cancer cell growth and motility. BMC Chem Biol. 2010; 10:5. [PubMed: 20444281]

Lewis JA, Scott SA, Lavieri R, Buck JR, Selvy PE, Stoops SL, Armstrong MD, Brown HA, Lindsley CW. Design and synthesis of isoform-selective phospholipase D (PLD) inhibitors. Part I: Impact of alternative halogenated privileged structures for PLD1 specificity. Bioorg Med Chem Lett. 2009; 19:1916–1920. [PubMed: 19268584]

Lin WW, Chen BC. Distinct PKC isoforms mediate the activation of cPLA2 and adenylyl cyclase by phorbol ester in RAW264.7 macrophages. Br J Pharmacol. 1998; 125:1601–1609. [PubMed: 9884090]

Manning G. Genomic overview of protein kinases. WormBook. 2005

Martina JA, Chen Y, Gucek M, Puertollano R. MTORC1 functions as a transcriptional regulator of autophagy by preventing nuclear transport of TFEB. Autophagy. 2012; 8:877–876.

Maurer K, Reyes-Robles T, Alonzo F, Durbin J, Torres VJ, Cadwell K. Autophagy Mediates Tolerance to Staphylococcus aureus Alpha-Toxin. Cell Host Microbe. 2015

McMullan R, Anderson A, Nurrish S. Behavioral and immune responses to infection require Gαq-RhoA signaling in C. elegans. PLoS Pathog. 2012; 8:e1002530. [PubMed: 22359503]

Medina DL, Di Paola S, Peluso I, Armani A, De Stefani D, Venditti R, Montefusco S, Scotto-Rosato A, Prezioso C, Forrester A, et al. Lysosomal calcium signalling regulates autophagy through calcineurin and TFEB. Nat Cell Biol. 2015; 17:288–299. [PubMed: 25720963]

Medzhitov R, Horng T. Transcriptional control of the inflammatory response. Nat Rev Immunol. 2009; 9:692–703. [PubMed: 19859064]

Monovich L, Mugrage B, Quadros E, Toscano K, Tommasi R, LaVoie S, Liu E, Du Z, LaSala D, Boyar W, et al. Optimization of halopemide for phospholipase D2 inhibition. Bioorg Med Chem Lett. 2007; 17:2310–2311. [PubMed: 17317170]

Navarro MN, Goebel J, Hukelmann JL, Cantrell DA. Quantitative phosphoproteomics of cytotoxic T cells to reveal protein kinase d 2 regulated networks. Mol Cell Proteomics MCP. 2014; 13:3544–3557. [PubMed: 25266776]

O'Rourke EJ, Ruvkun G. MXL-3 and HLH-30 transcriptionally link lipolysis and autophagy to nutrient availability. Nat Cell Biol. 2013; 15:668–676. [PubMed: 23604316]

Palmieri M, Impey S, Kang H, Di Ronza A, Pelz C, Sardiello M, Ballabio A. Characterization of the CLEAR network reveals an integrated control of cellular clearance pathways. Hum Mol Genet. 2011; 20:3852–3866. [PubMed: 21752829]

Park JE, Kim YI, Yi AK. Protein Kinase D1: A New Component in TLR9 Signaling. J Immunol. 2008; 181:2044–2055. [PubMed: 18641342]

Park JE, Kim YI, Yi AK. Protein kinase D1 is essential for MyD88-dependent TLR signaling pathway. J ImmunolBaltim Md 1950. 2009; 182:6316–6327.

Peña-Llopis S, Vega-Rubin-de-Celis S, Schwartz JC, Wolff NC, Tran TAT, Zou L, Xie XJ, Corey DR, Brugarolas J. Regulation of TFEB and V-ATPases by mTORC1. EMBO J. 2011; 30:3242–3258. [PubMed: 21804531]

Pfaffl MW. A new mathematical model for relative quantification in real-time RT-PCR. Nucleic Acids Res. 2001; 29:e45. [PubMed: 11328886]

Powell JR, Ausubel FM. Models of Caenorhabditis elegans infection by bacterial and fungal pathogens. Methods Mol Biol Clifton NJ. 2008; 415:403–427.

Ren M, Feng H, Fu Y, Land M, Rubin CS. Protein kinase D is an essential regulator of C. elegans innate immunity. Immunity. 2009; 30:521–532. [PubMed: 19371715]

Roczniak-Ferguson A, Petit CS, Froehlich F, Qian S, Ky J, Angarola B, Walther TC, Ferguson SM. The Transcription Factor TFEB Links mTORC1 Signaling to Transcriptional Control of Lysosome Homeostasis. Sci Signal. 2012; 5:ra42–ra42. [PubMed: 22692423]

Rozengurt E. Protein Kinase D Signaling: Multiple Biological Functions in Health and Disease. Physiology. 2011; 26:23–33. [PubMed: 21357900]

Samie M, Cresswell P. The transcription factor TFEB acts as a molecular switch that regulates exogenous antigen-presentation pathways. Nat Immunol. 2015 advance online publication.

Sardiello M, Palmieri M, Di Ronza A, Medina DL, Valenza M, Gennarino VA, Di Malta C, Donaudy F, Embrione V, Polishchuk RS, et al. A gene network regulating lysosomal biogenesis and function. Sci N Y NY. 2009; 325:473–477.

Scott SA, Selvy PE, Buck JR, Cho HP, Criswell TL, Thomas AL, Armstrong MD, Arteaga CL, Lindsley CW, Brown HA. Design of isoform-selective phospholipase D inhibitors that modulate cancer cell invasiveness. Nat Chem Biol. 2009; 5:108–117. [PubMed: 19136975]

Settembre C, Di Malta C, Polito VA, Garcia-Arencibia M, Vetrini F, Erdin S, Erdin SU, Huynh T, Medina D, Colella P, et al. TFEB links autophagy to lysosomal biogenesis. Sci N Y NY. 2011; 332:1429–1433.

Settembre C, De Cegli R, Mansueto G, Saha PK, Vetrini F, Visvikis O, Huynh T, Carissimo A, Palmer D, Klisch TJ, et al. TFEB controls cellular lipid metabolism through a starvation-induced autoregulatory loop. Nat Cell Biol. 2013; 15:647–658. [PubMed: 23604321]

Shapira SD, Hacohen N. Systems biology approaches to dissect mammalian innate immunity. Curr Opin Immunol. 2011; 23:71–77. [PubMed: 21111589]

Smith IM, Hoshi N. ATP competitive protein kinase C inhibitors demonstrate distinct state-dependent inhibition. PloS One. 2011; 6:e26338. [PubMed: 22043317]

Su W, Yeku O, Olepu S, Genna A, Park JS, Ren H, Du G, Gelb MH, Morris AJ, Frohman MA. 5-Fluoro-2-indolyl des-chlorohalopemide (FIPI), a phospholipase D pharmacological inhibitor that alters cell spreading and inhibits chemotaxis. Mol Pharmacol. 2009; 75:437–446. [PubMed: 19064628]

Taylor SJ, Chae HZ, Rhee SG, Exton JH. Activation of the β1 isozyme of phospholipase C by α subunits of the Gq class of G proteins. Nature. 1991; 350:516–518. [PubMed: 1707501]

Timmons L, Court DL, Fire A. Ingestion of bacterially expressed dsRNAs can produce specific and potent genetic interference in Caenorhabditis elegans. Gene. 2001; 263:103–112. [PubMed: 11223248]

Trieu A, Bokil N, Dunn JA, Roberts TL, Xu D, Liew FY, Hume DA, Stacey KJ, Sweet MJ. TLR9-independent effects of inhibitory oligonucleotides on macrophage responses to S. typhimurium. Immunol Cell Biol. 2009; 87:218–225. [PubMed: 19048019]

Van Engelenburg SB, Palmer AE. Imaging type-III secretion reveals dynamics and spatial segregation of Salmonella effectors. Nat Methods. 2010; 7:325–330. [PubMed: 20228815]

Vázquez-Manrique RP, Nagy AI, Legg JC, Bales OAM, Ly S, Baylis HA. Phospholipase C-ε Regulates Epidermal Morphogenesis in Caenorhabditis elegans. PLOS Genet. 2008; 4:e1000043. [PubMed: 18369461]

Visvikis O, Ihuegbu N, Labed SA, Luhachack LG, Alves AMF, Wollenberg AC, Stuart LM, Stormo GD, Irazoqui JE. Innate host defense requires TFEB-mediated transcription of cytoprotective and antimicrobial genes. Immunity. 2014; 40:896–909. [PubMed: 24882217]

Wong C, Jin ZG. Protein Kinase C-dependent Protein Kinase D Activation Modulates ERK Signal Pathway and Endothelial Cell Proliferation by Vascular Endothelial Growth Factor. J Biol Chem. 2005; 280:33262–33269. [PubMed: 16006559]

Wu-zhang AX, Newton AC. Protein kinase C pharmacology: refining the toolbox. Biochem J. 2013; 452:195–209. [PubMed: 23662807]

Ziegler K, Kurz CL, Cypowyj S, Couillault C, Pophillat M, Pujol N, Ewbank JJ. Antifungal innate immunity in C. elegans: PKCdelta links G protein signaling and a conserved p38 MAPK cascade. Cell Host Microbe. 2009; 5:341–352. [PubMed: 19380113]

Zou CG, Tu Q, Niu J, Ji XL, Zhang KQ. The DAF-16/FOXO transcription factor functions as a regulator of epidermal innate immunity. PLoS Pathog. 2013; 9:e1003660. [PubMed: 24146615]

Zugasti O, Bose N, Squiban B, Belougne J, Kurz CL, Schroeder FC, Pujol N, Ewbank JJ. Activation of a G protein-coupled receptor by its endogenous ligand triggers the innate immune response of Caenorhabditis elegans. Nat Immunol. 2014; 15:833–838. [PubMed: 25086774]

Highlights

- Protein Kinase D (PKD) is necessary and sufficient for TFEB activation.
- Phospholipase C (PLC) acts upstream of PKD and TFEB in response to infection.
- Nematode Gαq functions upstream of PLC.
- Knockdown of the gene encoding PKD1 results in defective TFEB activation.

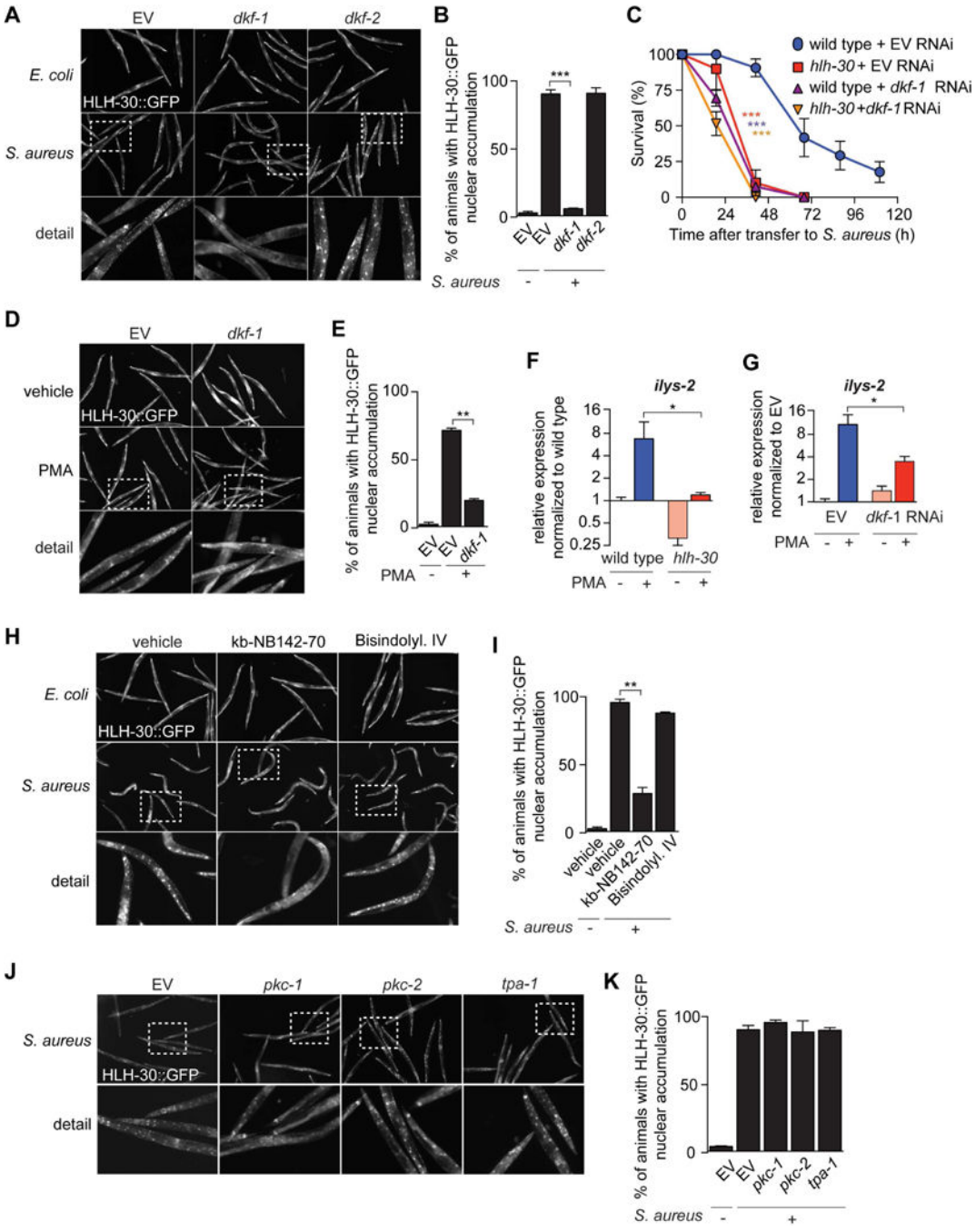

Figure 1. DKF-1/PKD is necessary and sufficient for HLH-30/TFEB activation

(A) HLH-30::GFP animals were reared on *E. coli* carrying empty vector (EV), *dkf-1* RNAi, or *dkf-2* RNAi, and subsequently fed with *E. coli* OP50 (top row) or infected with *S. aureus* (middle row). Shown are representative epifluorescence micrographs. Hatched boxes indicate areas enlarged in *detail* (Bottom Row). **(B)** Quantitative analysis. Data are mean ± SEM (two biological replicates, n ≥ 50 per condition). *** p ≤ 0.001 (two-sample *t* test). **(C)** Survival of wild type and *hlh-30* mutant animals reared on *E. coli* carrying *dkf-1* RNAi or empty vector control prior to infection with *S. aureus*. *** p ≤ 0.001 (Log-Rank test). **(D)**

Animals were treated with *dkf-1* RNAi as in (A) and subsequently incubated with 1 μg/ml PMA for 30 min. Shown are representative epifluorescence micrographs (middle row). Hatched boxes indicate areas enlarged in *detail* (bottom row). Top row shows animals treated with vehicle. **(E)** Quantitative analysis. Data are mean ± SEM (two biological replicates, n ≥ 50 per condition). ** p ≤ 0.01 (two-sample *t* test). **(F)** qRT-PCR of *ilys-2* in wild type or *hlh-30* mutants. Animals were incubated with 1 μg/ml PMA for 8 h. Results are normalized to control wild type animals. Data are mean ± SEM (three biological replicates, three technical replicates, n ≥ 3,000 per condition). **(G)** qRT-PCR of *ilys-2* in worms reared on *E. coli* carrying empty vector control or *dkf-1* RNAi. Animals were incubated with 1 μg/ml PMA for 8 h. Results are normalized to empty vector control. * p ≤ 0.05 (two-sample *t* test). **(H)** HLH-30::GFP animals were treated with kb-NB142-70 or Bisindolylmaleimide IV, and subsequently fed with *E. coli* OP50 (top row) or infected with *S. aureus* (middle row). Shown are representative epifluorescence micrographs. Hatched boxes indicate areas enlarged in *detail* (Bottom Row). **(I)** Quantitative analysis. Data are mean ± SEM (two biological replicates, n ≥ 50 per condition). ** p ≤ 0.01 (two-sample *t* test). **(J)** HLH-30::GFP animals were reared on *E. coli* carrying empty vector (EV), *pkc-1*, *pkc-2*, or *tpa-1* RNAi, and subsequently infected with *S. aureus* (top row). Shown are representative epifluorescence micrographs. Hatched boxes indicate areas enlarged in *detail* (bottom row). **(K)** Quantitative analysis. Data are mean ± SEM (three biological replicates, n ≥ 50 per condition). See also Figure S1.

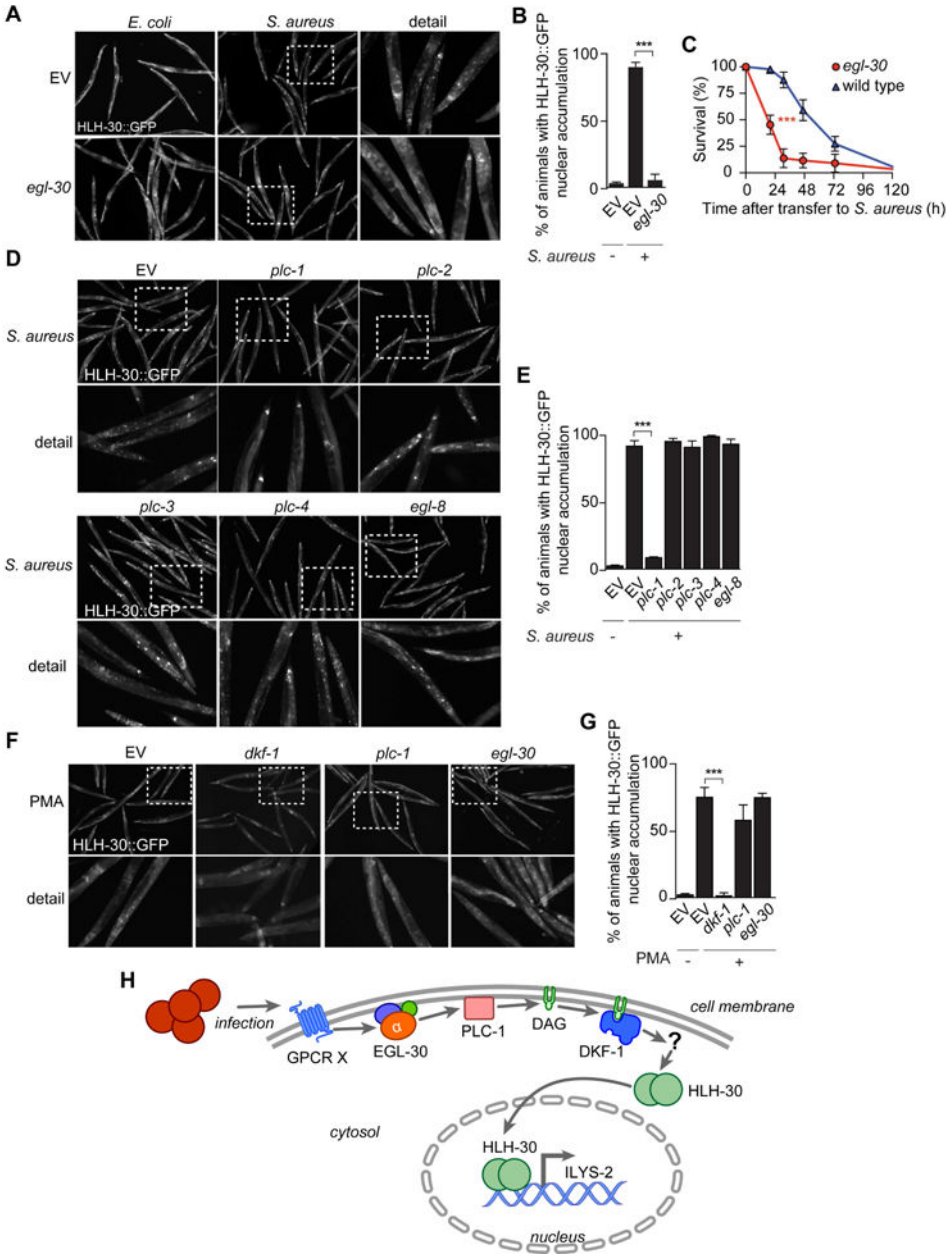

Figure 2. A Gα$_q$-PLCε-PKD pathway controls TFEB in *C. elegans*

(A) HLH-30::GFP animals were reared on *E. coli* carrying empty vector or *egl-30* RNAi, and subsequently infected with *S. aureus*. Shown are representative epifluorescence micrographs. Hatched boxes indicate areas enlarged in *detail*. EV, empty vector control RNAi. **(B)** Quantitative analysis. Data are mean ± SEM (two biological replicates, n ≥ 50 per condition). *** p ≤ 0.001 (two-sample *t* test). **(C)** Survival of wild type and *egl-30* mutant animals infected with *S. aureus*. *** p ≤ 0.001 (Log-Rank test). **(D)** HLH-30::GFP animals were reared on *E. coli* carrying empty vector or *plc-1, plc-2, plc-3, plc-4*, or *egl-8* RNAi, and subsequently infected with *S. aureus*. Shown are representative epifluorescence micrographs. **(E)** Quantitative analysis. Data are mean ± SEM (two biological replicates, n ≥ 50 per condition). *** p ≤ 0.001 (two-sample *t* test). **(F)** Animals were treated with *dkf-1*,

plc-1, or *egl-30* RNAi and subsequently incubated with 1 μg/ml PMA for 30 min. Shown are representative epifluorescence micrographs (top row). Hatched boxes indicate areas enlarged in *detail* (bottom row). **(G)** Quantitative analysis. Data are mean ± SEM (two biological replicates, $n \geq 50$ per condition). *** $p \leq 0.001$ (two-sample *t* test). **(H)** Proposed hypothetical model for HLH-30 regulation by infection.

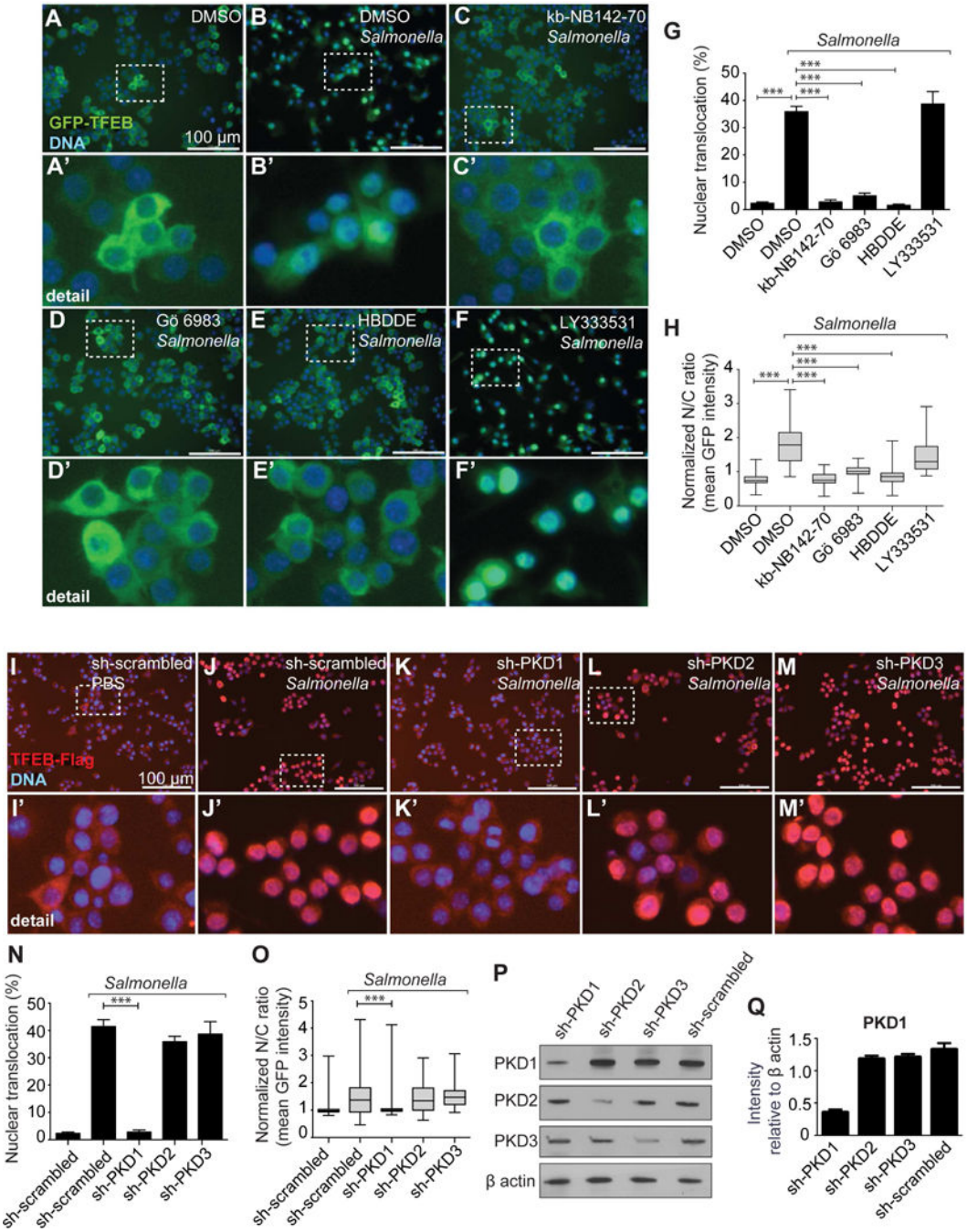

Figure 3. PKD1 and PKCα/γ are necessary for activation of TFEB by infection

TFEB-GFP RAW264.7 cells were preincubated with PKC and PKD inhibitors for 1 h previous to infection with *S. enterica* (MOI = 100) for 2 h. Shown are representative images from one replicate, and quantification of three biological replicates of three technical replicates each. (**A**) DMSO control. (**A′**) detail. (**B**) *S. enterica* SL1344. (**B′**) detail. (**C**) 10 μM kb-NB142-70 (PKD inhibitor). (**C′**) detail. (**D**) 5 μM Gö 6983 (pan-PKC inhibitor). (**D′**) detail. (**E**) 1 mM HBDDE (selective inhibitor of PKCα and PKCγ). (**E′**) detail. (**F**) 10 μM LY333531 (selective inhibitor of PKCβ1 and PKCβ2). (**F′**) detail. (**G**) Percentage of cells

with nuclear translocation was measured with Gen5 analysis software. (**H**) GFP intensity in nucleus compared to cytoplasm (N/C ratio) was measured using CellProfiler. See *Methods* for details. ** $p \leq 0.01$, *** $p \leq 0.001$ (one-way ANOVA followed by Tukey's post-hoc test). Scale bars = 100 μm. (**I–M′**) TFEB-Flag RAW264.7 cells were infected with *Salmonella* after shRNA treatment. Shown are anti-FLAG immunofluorescence micrographs. Scale bars = 100 μm. (**I**) scrambled shRNA control with PBS. (**I′**) detail. (**J**) scrambled shRNA control with *S. enterica* SL1344. (**J′**) detail. (**K**) PKD1 shRNA with *S. enterica* SL1344. (**K′**) detail. (**L**) PKD2 shRNA with *S. enterica* SL1344. (**L′**) detail. (**M**) PKD3 shRNA with *S. enterica* SL1344. (**M′**) detail. (**N**) Percentage of cells with nuclear translocation. (**O**) GFP intensity in nucleus compared to cytoplasm (N/C ratio). ** $p \leq 0.01$, *** $p \leq 0.001$ (one-way ANOVA followed by Tukey's post-hoc test). (**P**) Anti- PKD1, PKD2, PKD3, and β actin immunoblots of lysates from sh-PKD1, sh-PKD2, sh-PKD3, and scrambled control cells. (**Q**) Quantitative analysis of PKD1 immunoblot, normalized to β actin loading control. See also the Figure S2.

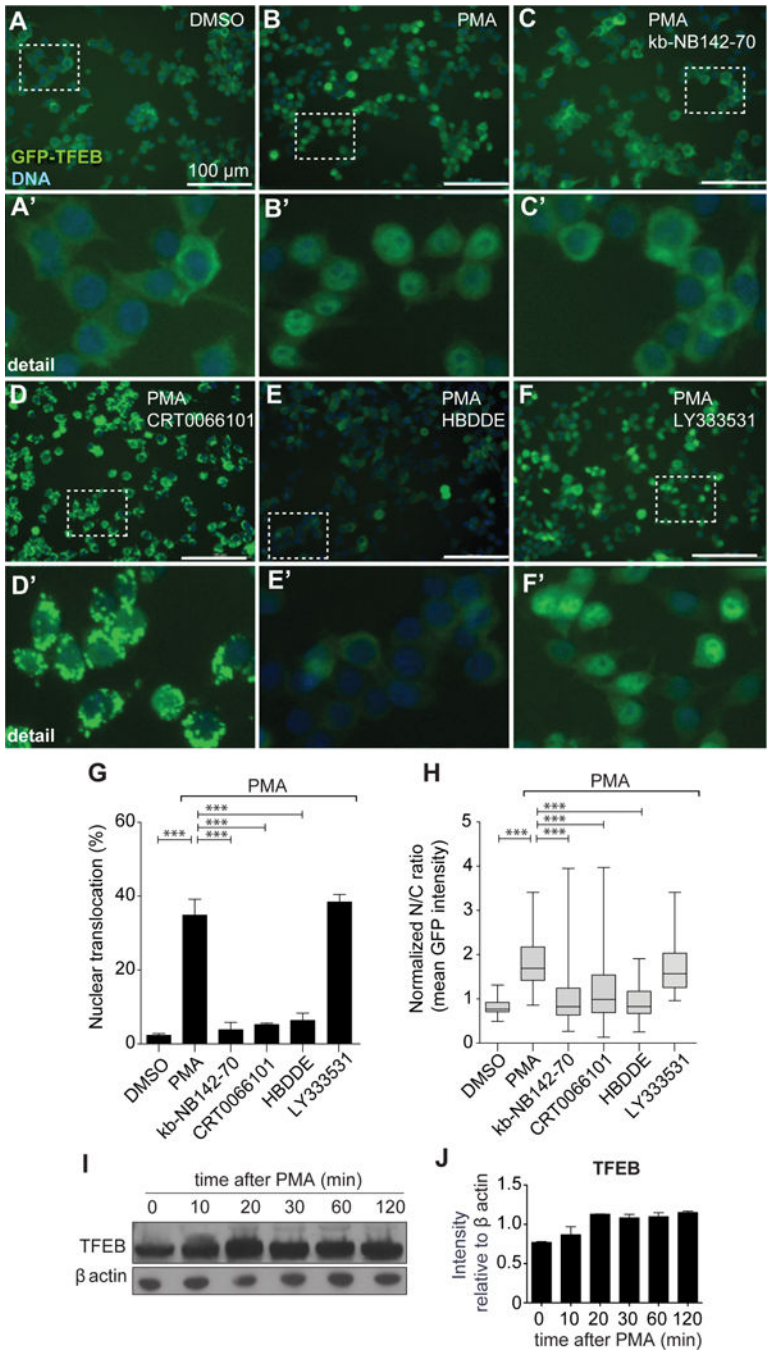

Figure 4. Activation of PKC or PKD is sufficient for TFEB activation

TFEB-GFP RAW264.7 cells were preincubated with inhibitors for 1 h previous to addition of 100 ng/ml PMA for 30 min. Shown are representative images from one replicate, and quantification of three biological replicates of three technical replicates each. (**A**) DMSO control. (**A′**) detail. (**B**) DMSO plus PMA. (**B′**) detail. (**C**) 10 μM kb-NB142-70 (specific PKD inhibitor). (**C′**) detail. (**D**) 5 μM CRT0066101 (specific PKD inhibitor). (**D′**) detail. (**E**) 1 mM HBDDE (selective inhibitor of PKCα and PKCγ). (**E′**) detail. (**F**) 10 μM LY333531 (PKCβ1 and PKCβ2 inhibitor). (**F′**) detail. Scale bars = 100 μm. (**G**) Percentage of cells with

nuclear translocation was measured with Gen5 analysis software. (**H**) GFP intensity in nucleus compared to cytoplasm (N/C ratio) was measured using CellProfiler. Please see *Methods* for more detail. ** $p \leq 0.01$, *** $p \leq 0.001$ (One-way ANOVA followed by Tukey's post-hoc test). (**I**) Images from immunoblot following addition of 100 ng/ml PMA, primary antibodies are indicated on the left. (**J**) Quantitative analysis of TFEB immunoblot, normalized to β actin loading control. See also the Figure S3.

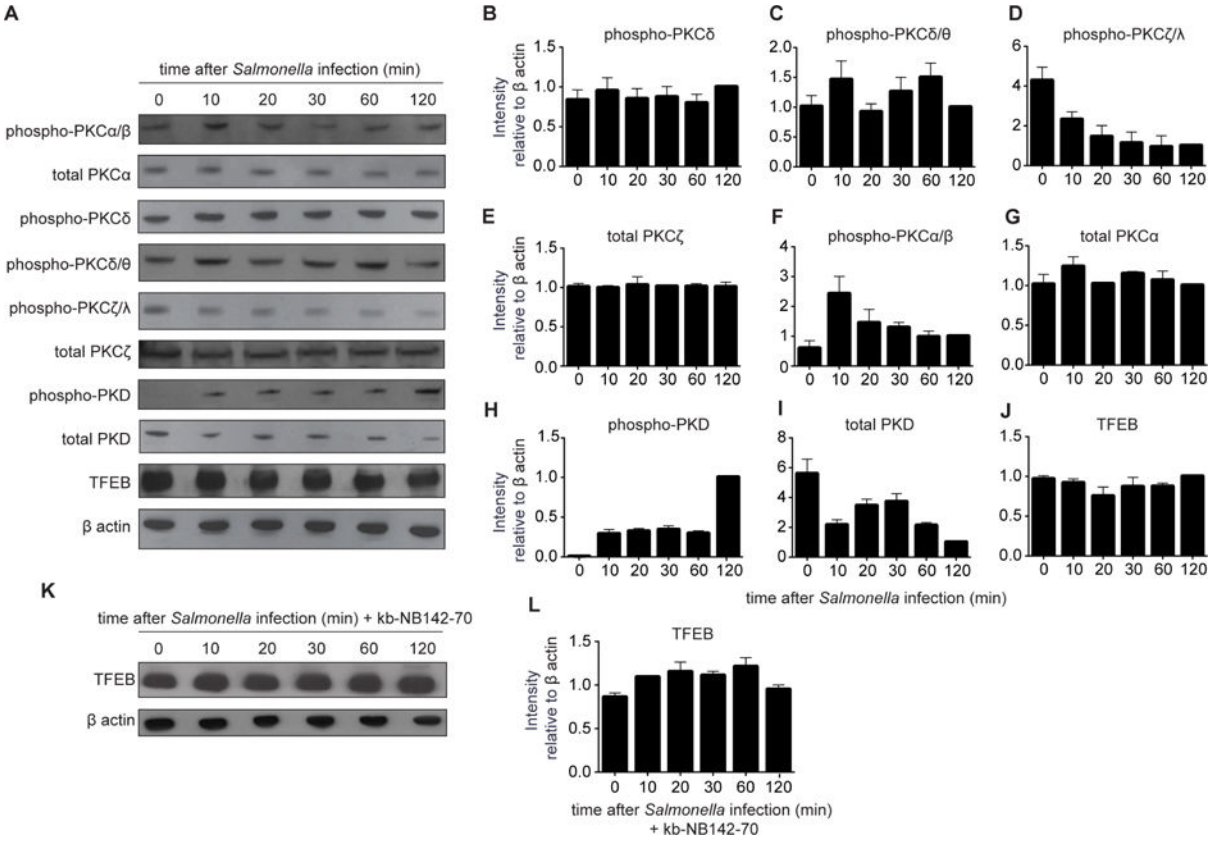

Figure 5. PKD and PKCα are quickly activated after infection

(**A–N**) RAW264.7 cells were infected with *S. enterica* SL1344 (MOI = 100) for 0 (control), 10, 20, 30, 60, and 120 min, lysed, and subjected to immunoblot analysis. Shown are representative results from three biological replicates. (**A**) Images from immunoblots. Primary antibodies are indicated on the left. (**B–J**) Quantitative analysis, normalized to β actin loading control. (**K**) Images from immunoblots after *Salmonella* infection plus 10 μM kb-NB142-70 (specific PKD inhibitor). Primary antibodies are indicated on the left. (**L**) Quantitative analysis, normalized to β actin loading control.

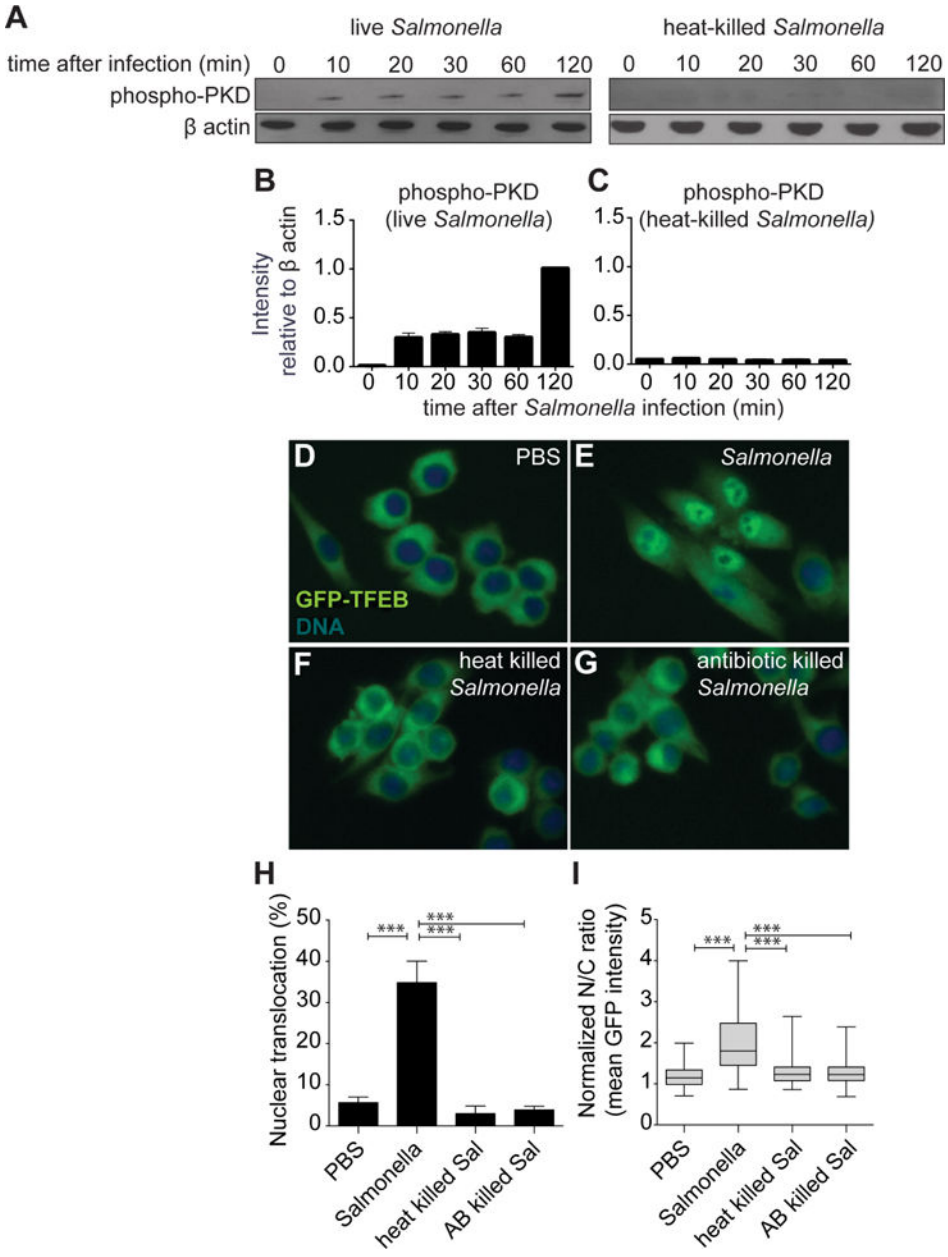

Figure 6. *Salmonella enterica* must be alive to activate the PKD-TFEB pathway in macrophages

(A) Anti-phospho-PKD immunoblot. RAW264.7 cells were incubated with live or dead *S. enterica* SL1344 (MOI = 100) for 0 (control), 10, 20, 30, 60, and 120 min, lysed, and subjected to immunoblot analysis. **(B,C)** Quantitative analysis, normalized to β actin loading control. **(D–G)** TFEB-GFP RAW264.7 cells were incubated with live or dead *S. enterica* (MOI = 100) for 2 h. For heat killed condition, bacteria were heated to 75 °C for 1 h and 100% killing was confirmed by culture for 48 h on LB-streptomycin agar at 37°C. For antibiotic-killed bacteria, gentamicin (100 μg/ml) was added to washed bacteria in PBS for 2 h and 100% killing was confirmed by culture for 48 h on LB-streptomycin agar at 37°C. Shown are representative images from one replicate, and quantification of three biological replicates of three technical replicates each. **(D)** PBS control. **(E)** Live *S. enterica* SL1344.

(F) Heat-killed *S. enterica*. **(G)** Antibiotic-killed *S. enterica*. **(H)** Percentage of cells with nuclear translocation was measured with Gen5 analysis software. **(I)** GFP intensity in nucleus compared to cytoplasm (N/C ratio) was measured using CellProfiler. ** $p \leq 0.01$, *** $p \leq 0.001$ (one-way ANOVA followed by Tukey's post-hoc test).

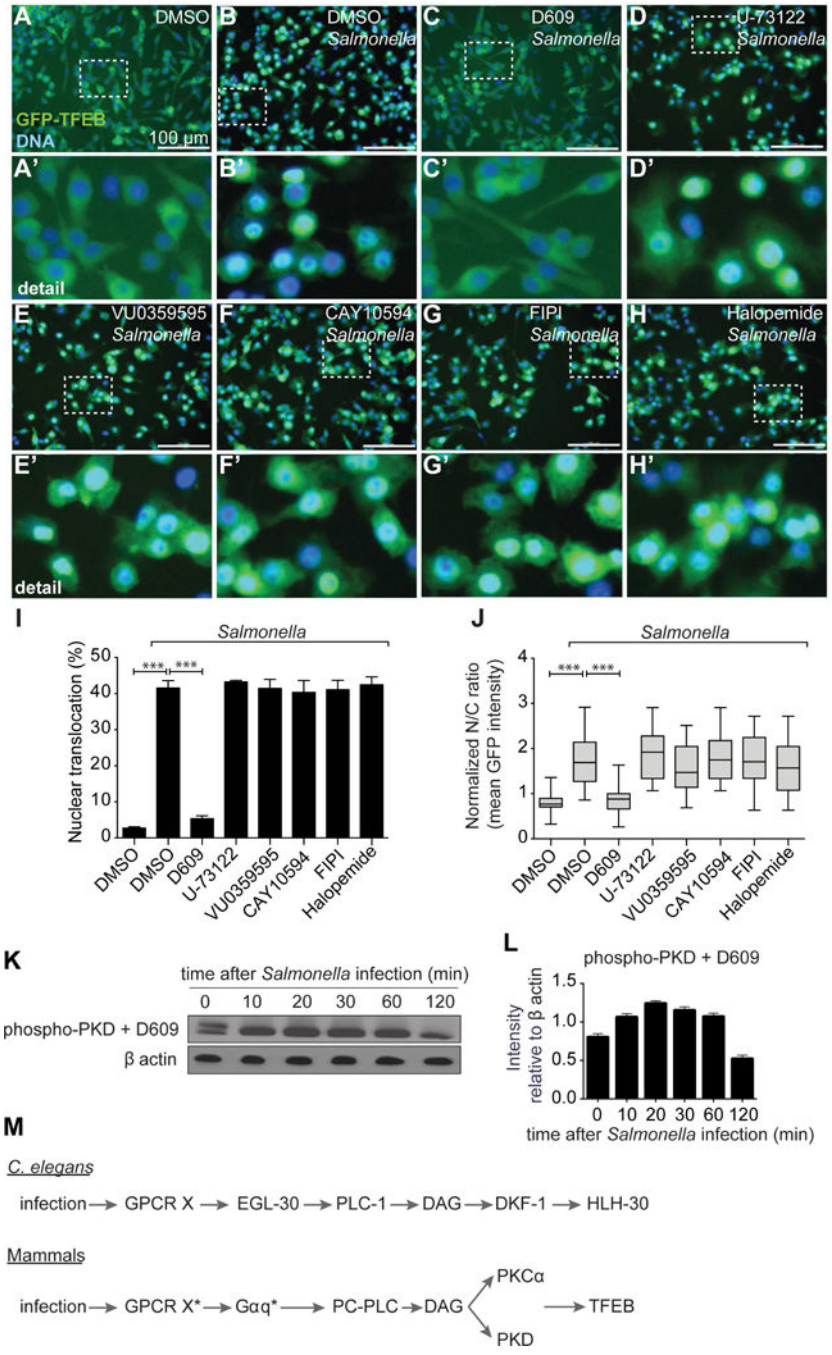

Figure 7. PC-PLC activity is required for TFEB activation by infection

TFEB-GFP RAW264.7 cells were preincubated with PLC inhibitors for 1 h prior to infection with *S. enterica* (MOI = 100) for 2 h. Shown are representative images from one replicate, and quantification of three biological replicates of three technical replicates each. Scale bars = 100 μm. (**A**) DMSO control. (**A′**) detail. (**B**) *S. enterica* SL1344. (**B′**) detail. (**C**) 50 μM tricyclodecan-9-yl-xanthogenate (D609), which inhibits phosphatidylcholine-specific phospholipase C (PC-PLC). (**C′**) detail. (**D**) 50 μM U-73122, which inhibits phosphoinositide-specific phospholipase C (PI-PLC). (**D′**) detail. (**E**) 10 μM VU0359595,

which inhibits phospholipase D1 (PLD1). (**E′**) detail. (**F**) 10 μM CAY10594, which inhibits phospholipase D2 (PLD2). (**F′**) detail. (**G**) 10 μM FIPI, which inhibits PLD1 and PLD2. (**G′**) detail. (**H**) 10 μM halopemide, which inhibits PLD1 and PLD2. (**H′**) detail. (**I**) Percentage of cells with nuclear translocation was measured with Gen5 analysis software. (**J**) GFP intensity in nucleus compared to cytoplasm (N/C ratio) was measured using CellProfiler. ** $p \leq 0.01$, *** $p \leq 0.001$ (One-way ANOVA followed by Tukey's post-hoc test). (**K,L**) RAW264.7 cells were incubated with 50 μM D609 for 1 hour and then infected with *S. enterica* SL1344 (MOI = 100) for 0 (control), 10, 20, 30, 60, and 120 min, lysed, and subjected to immunoblot analysis. Shown are representative results from three biological replicates. (**K**) Images from immunoblots. Primary antibodies are indicated on the left. (**L**) Quantitative analysis, normalized to β actin loading control. (**M**) Proposed genetic pathways for signal transduction and activation of TFEB in *C. elegans* and mammals by infection. * denotes mammalian steps proposed by analogy with *C. elegans*.